Rock and Soil Mechanics

Volume 43 | Issue 5 Article 6

7-4-2022

Experimental study of regulation performance of open flexible debris flow barriers

Dong-po WANG
State Key Laboratory of Geohazard Prevention and Geoenvironment Protection, Chengdu University of Technology, Chengdu, Sichuan 610059, China

Jun ZHAO
State Key Laboratory of Geohazard Prevention and Geoenvironment Protection, Chengdu University of Technology, Chengdu, Sichuan 610059, China

Xiao-mei ZHANG
Sichuan Province Geological Engineering Co. Ltd., Chengdu, Sichuan 610031, China

Xin YANG
State Key Laboratory of Geohazard Prevention and Geoenvironment Protection, Chengdu University of Technology, Chengdu, Sichuan 610059, China

Custom Citation

WANG Dong-po, ZHAO Jun, ZHANG Xiao-mei, YANG Xin, . Experimental study of regulation performance of open flexible debris flow barriers[J]. Rock and Soil Mechanics, 2022, 43(5): 1237-1248.

Rock and Soil Mechanics 2022 43(5): 1237−1248 ISSN 1000−7598
https: //doi.org/10.16285/j.rsm.2021.6248 rocksoilmech.researchcommons.org/journal

Experimental study of regulation performance of open flexible debris flow barriers

WANG Dong-po[1], ZHAO Jun[1], ZHANG Xiao-mei[2], YANG Xin[1]

1. State Key Laboratory of Geohazard Prevention and Geoenvironment Protection, Chengdu University of Technology, Chengdu, Sichuan 610059, China

2. Sichuan Province Geological Engineering Co. Ltd., Chengdu, Sichuan 610031, China

Abstract: Flexible debris flow barriers are important engineering measures to prevent debris flow disasters. The existing prevention structures are mainly in the form of closed barriers, which are prone to blockage with poor regulation abilities. Therefore, we proposed open flexible debris flow barriers to overcome the above shortcomings. Based on theoretical analyses and physical model tests, the research on the regulation performance of the open flexible debris flow barriers was carried out, and the theoretical formulas for the velocity attenuation rate, run-up height, and blocking rate of debris flows were deduced. The results show that compared with the closed flexible debris flow barriers, the improved structure has a good self-cleaning effect and can effectively control the peak velocity of debris flows. The calculation results through the derived non-dimensional theoretical formulas are in good agreement with the physical test results. The velocity attenuation rate, run-up height, and blocking rate of debris flows are mainly controlled by the relative open height, dimensionless flow depth, relative density of debris flows, and the Froude number. The velocity attenuation rate and blocking rate are negatively correlated with the relative open height, and positively correlated with the relative density of debris flows. The run-up height is negatively correlated with both the relative open height and the relative density. The above research can provide theoretical and technical support for the application of open flexible barriers in debris flow prevention and control projects.

Keywords: debris flow; open flexible debris flow barriers; velocity attenuation rate; run-up height; blocking rate

1 Introduction

Flexible barriers are commonly adopted to prevent geohazards due to their advantages in safety, low cost, and environmental friendliness[1−2]. In recent years, flexible barriers have exhibited significant effects in preventing debris flows, and they have been increasingly employed to mitigate debris flows in high or narrow steep gullies with a river width less than 30 m[3−4]. According to field investigation and literature review[5−8], well-developed standards for designing flexible debris flow barriers are still unavailable, and many problems, such as the siltation behind the barriers resulting in the loss of regulation on debris flows (Fig.1), still exist in controlling debris flows using flexible barriers.

Fig. 1 Flexible debris flow barriers[6]

The study of flexible debris flow barriers is concentrated on the dynamic response of flexible debris flow barriers to the impact of debris flows. Wendeler et al.[6, 8] and Volkwein et al.[9] employed flexible barriers to successfully intercept the debris flows with a volume of 1.9×10^4 m^3, and they quantified the relationship between the mesh diameter of the flexible barriers and the grain size of the debris material through flume experiments. The experimental findings demonstrated that the optimal retention was achieved using the barrier net with a mesh size equal to d_{90} grain size. Tan et al.[10] developed a new model to calculate the impact load on the flexible barriers overflowed by debris flows by taking the siltation behind the barriers into account. Wang and Zhang[11], Armanini et al.[12], and Song et al.[13] deduced the theoretical formulas for the impact load and the run-up height of debris flows under different barrier structures based on conservation equations. Wang et al.[14−16] simulated the movement processes of the boulders in debris flows impacting flexible barriers, and they investigated the influences of the debris material' mass and velocity as well as the flexible barriers' structural characteristics on the dynamic response of barriers. Based on the computational fluid dynamics-discrete element method (CFD-DEM) coupled framework, Li et al.[17] explored the deformation and failure mechanisms of flexible barriers under the impact of debris flows. By performing specially designed flume experiments, Li et al.[18] and Sun et al.[19] obtained empirical expressions to assess the performance of check dams on trapping sediments and regulating debris flows. Wang et al.[20] and Yu et al.[21] conducted the numerical

Received: 07 August 2021 Revised: 19 November 2021
This work was supported by the National Natural Science Foundation of China (41877266) and the Science Foundation for Distinguished Young Scholars of Sichuan Province (2020JDJQ0044).
First author: WANG Dong-po, male, born in 1984, PhD, Postdoc, Professor, PhD supervisor, research interests: impact dynamics of geohazards. E-mail: wangdongpo@cdut.edu.cn

simulation to investigate the influence of the barriers' opening parameters on the flow amounts of debris flows and further proposed the corresponding optimization strategy for the opening parameters. The aforementioned research mainly focused on the traditional closed flexible barriers, and the research on the regulation performance of open flexible debris flow barriers is still at infancy until now.

The traditional closed flexible barriers were optimized into the open flexible barriers (Fig. 2) in this paper, aiming at shaving the peak flow amount of debris flows and mitigating the siltation after the barriers (Fig. 3). Based on the dimensional analysis method [22–24] and physical model tests, the correlations between the main factors, such as the open height of flexible barriers, the density of debris flows, the velocity attenuation rate of debris flows, the blocking rate of flexible barriers, and the run-up height of debris flows were clarified, and the regulation performance of open flexible debris flow barriers was investigated.

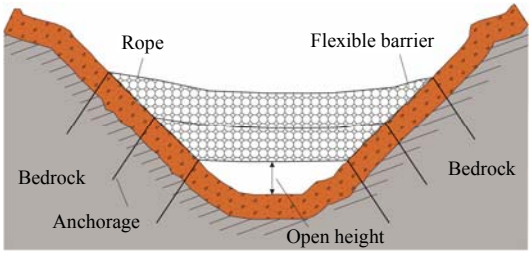

Fig. 2 Open flexible debris flow barriers

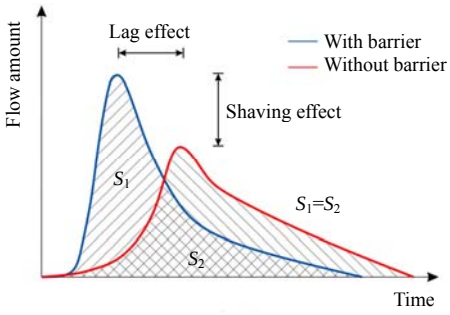

Fig. 3 Shaving effect of debris flow peak

2 Theoretical calculation

The interaction between debris flows and open flexible barriers are controlled by multiple factors, including the open height a, the mesh size (diagonal distance of square hexagon) b, the debris flow velocity before barriers u_0, the debris flow depth before barriers h, the density of debris flows ρ, the solid phase density of debris flows ρ_s, the characteristic grain size of debris flows d, the run-up height of debris flows H, the initial volume of debris flows V, the longitudinal slope of the gully θ, and the gravitational acceleration g. During the theoretical calculation of debris flows impacting open flexible barriers, the movement processes of debris flows were appropriately simplified: the characteristic grain size and total discharge volume of debris flows kept constant; the debris flow velocity was uniform and continuous along the depth direction (u_0 represents the velocity of the longitudinal section); and the debris flow depth remained constant within the same cross section.

2.1 Formulas for velocity attenuation rate of debris flows and blocking rate of flexible barriers

The movement processes of debris flows impacting open flexible barriers were analyzed, and the evaluation index of the regulation performance of open flexible debris flow barriers R was then regarded as a function of eight influencing factors (a, b, h, u_0, θ, g, ρ, and ρ_s):

$$R = f(a,b,h,u_0,\theta,g,\rho,\rho_s) \tag{1}$$

The peak flow amount and the overall amount of overflow are crucial design bases in the debris flow prevention engineering, but the experimental data such as the debris flow depth behind the barriers are difficult to gather. In order to reflect the prevention ability of flexible barriers against debris flow disasters, the velocity attenuation rate of debris flows R_a and the blocking rate of flexible barriers R_b were used as the evaluation indexes of the regulation performance of open flexible debris flow barriers. The dimensions of relevant physical parameters are summarized in Table 1.

Table 1 Parameter dimensions

Parameter	Symbol	Dimension
Open height	a	[L]
Mesh size	b	[L]
Debris flow depth before barriers	h	[L]
Debris flow velocity before barriers	u_0	$[L][T]^{-1}$
Longitudinal slope of gully	θ	1
Gravitational acceleration	g	$[L][T]^{-2}$
Density of debris flows	ρ	$[M][L]^{-3}$
Solid phase density of debris flows	ρ_s	$[M][L]^{-3}$
Velocity attenuation rate of debris flows	R_a	1
Blocking rate of flexible barriers	R_b	1
Run-up height of debris flows	H	[L]

Note: M, L, and T represent the dimensions of mass, length, and time, respectively.

The parameters in Eq. (1) can be classified into two categories: dimensionless parameters θ and dimensional parameters a, b, u_0, h, ρ, ρ_s, g. If the parameters themselves are dimensionless, they will not participate in the nondimensionalization process of other relevant parameters, which implies that the effect of θ in Eq. (1) can be temporarily ignored. The remaining seven parameters (number of parameters $n = 7$) in Eq. (1) include three basic parameters ($m = 3$), i.e., the time dimension T, the length dimension L, and the mass dimension M. According to the Π theorem[25] (Buckingham's theorem), these seven dimensional parameters can be represented by the three independent basic parameters, namely, $\pi = n - m = 4$. Therefore,

the regulation performance of open flexible debris flow barriers can be described as follows:

$$\Pi = f(\pi_1, \pi_2, \pi_3, \pi_4) \tag{2}$$

where Π depicts the dynamic processes of debris flows impacting flexible barriers, and π_1, π_2, π_3, and π_4 are independent dimensionless similar parameters.

Based on the dimensional analysis method, the form of the function *f* in Eq. (1) is determined as

$$R = x_0 a^{x_1} b^{x_2} h^{x_3} u_0^{x_4} g^{x_5} \rho^{x_6} \rho_s^{x_7} \tag{3}$$

where x_0 is the dimensionless scaling coefficient, and x_1, x_2, x_3, x_4, x_5, x_6, and x_7 are the coefficients to be determined for each variable. The dimension form of Eq. (3) is

$$\begin{aligned}&\dim(\mathrm{M}^0\mathrm{L}^0\mathrm{T}^0) = \\ &\dim[x_0(\mathrm{L})^{x_1}(\mathrm{L})^{x_2}(\mathrm{L})^{x_3}(\mathrm{LT}^{-1})^{x_4}(\mathrm{LT}^{-2})^{x_5}(\mathrm{ML}^{-3})^{x_6}(\mathrm{ML}^{-3})^{x_7}]\end{aligned} \tag{4}$$

Based on the principle of dimensional consistency, Eq. (4) is nondimensionalized and transformed into the basic solution vectors of the homogeneous linear equations $\boldsymbol{A}^{\mathrm{T}}\boldsymbol{X} = \boldsymbol{0}$:

$$\boldsymbol{A}^{\mathrm{T}}\boldsymbol{X} = \begin{bmatrix} 0 & 0 & 0 & 0 & 0 & 1 & 1 \\ 1 & 1 & 1 & 1 & 1 & -3 & -3 \\ 0 & 0 & 0 & -1 & -2 & 0 & 0 \end{bmatrix} \begin{bmatrix} x_1 \\ \vdots \\ x_7 \end{bmatrix} = \boldsymbol{0} \tag{5}$$

where $\boldsymbol{A}^{\mathrm{T}}$ is the dimensional matrix and $\boldsymbol{X}$ is the column vector of the coefficients to be determined. Let the basic solution system of Eq. (5) be $\boldsymbol{\varepsilon}_1 = [x_1, x_3, x_5, x_7]$, and the following solution can be then acquired:

$$\begin{aligned}\begin{bmatrix} x_2 \\ x_4 \\ x_6 \end{bmatrix} &= \begin{bmatrix} -1 & -1 & 1 & 0 \\ 0 & 0 & -2 & 0 \\ 0 & 0 & 0 & -1 \end{bmatrix} \boldsymbol{\varepsilon}_1 = \\ &\begin{bmatrix} -1 & -1 & 1 & 0 \\ 0 & 0 & -2 & 0 \\ 0 & 0 & 0 & -1 \end{bmatrix} \begin{bmatrix} x_1 \\ x_3 \\ x_5 \\ x_7 \end{bmatrix}\end{aligned} \tag{6}$$

Equation (6) is equivalent to

$$\left.\begin{aligned} x_2 &= x_5 - x_3 - x_1 \\ x_4 &= -2x_5 \\ x_6 &= -x_7 \end{aligned}\right\} \tag{7}$$

Substituting Eq. (7) into Eq. (3), we can get

$$R = x_0 a^{x_1} b^{x_5 - x_3 - x_1} h^{x_3} u_0^{-2x_5} g^{x_5} \rho^{-x_7} \rho_s^{x_7} \tag{8}$$

Eq. (8) can be reorganized as

$$R = x_0 \left(\frac{a}{b}\right)^{x_1} \left(\frac{h}{b}\right)^{x_3} \left(\frac{bg}{u_0^2}\right)^{x_5} \left(\frac{\rho_s}{\rho}\right)^{x_7} \tag{9}$$

By transforming the relevant variables in Eq. (9) into the Froude number form describing the mobility of debris flows, we can obtain

$$\begin{aligned} R &= \lambda_0 \left(\frac{a}{b}\right)^{\lambda_1} \left(\frac{h}{b}\right)^{\lambda_2} \left(\frac{u_0}{\sqrt{gb}}\right)^{\lambda_3} \left(\frac{\rho}{\rho_s}\right)^{\lambda_4} = \\ &\lambda_0 \left(\frac{a}{b}\right)^{\lambda_1} \left(\frac{h}{b}\right)^{\lambda_2} (\mathrm{Fr}_1)^{\lambda_3} (\rho')^{\lambda_4} \end{aligned} \tag{10}$$

where λ_0 is the dimensionless scaling coefficient; λ_1, λ_2, λ_3, and λ_4 are the coefficients to be determined; a/b is the relative open height of flexible barriers; h/b is the dimensionless debris flow depth; $\mathrm{Fr}_1 = u_0/(gb)^{0.5}$, is the Froude number[26]; and $\rho' = \rho/\rho_s$, is the relative density of debris flows.

2.2 Formulas for run-up height of debris flows

The design height of open flexible barriers is determined by the run-up height of debris flows *H*. The run-up height of debris flows is dominated by various parameters including the open height *a*, the mesh size *b*, the debris flow depth before barriers *h*, the debris flow velocity before barriers u_0, the longitudinal slope of the gully θ, the gravitational acceleration *g*, the density of debris flows ρ, and the solid phase density of debris flows ρ_s. The relationship between the run-up height of debris flows *H* and other physical parameters can be expressed as follows:

$$f(a, b, h, u_0, \theta, g, \rho, \rho_s, H) = 0 \tag{11}$$

From Eq. (11), the function characterizing the run-up height of debris flows *H* contains nine variables ($n = 9$). Select *b*, u_0, and ρ as the basic parameters ($m = 3$), six dimensionless π numbers can be therefore obtained, that is, $\pi = n - m = 6$. Since θ is a dimensionless variable, namely, it is naturally a π number:

$$\pi_1 = \theta \tag{12}$$

Establish the dimensional equation to figure out the second π number, and we can get

$$\pi_2 = b^{p_2} u_0^{q_2} \rho^{r_2} a \tag{13}$$

where p_2, q_2, and r_2 are the coefficients to be determined for each variable. According to the principle of dimensional consistency, Eq. (13) is nondimensionalized as

$$\dim(\mathrm{M}^0\mathrm{L}^0\mathrm{T}^0) = \dim[(\mathrm{L})^{p_2}(\mathrm{LT}^{-1})^{q_2}(\mathrm{ML}^{-3})^{r_2}\mathrm{L}] \tag{14}$$

The second π number was obtained as

$$\pi_2 = \frac{a}{b} \tag{15}$$

Similarly, other π numbers are figured out in turn as follows:

$$\pi_3 = \frac{h}{b}, \quad \pi_4 = \frac{u_0}{\sqrt{bg}}, \quad \pi_5 = \frac{\rho}{\rho_s}, \quad \pi_6 = \frac{H}{b} \tag{16}$$

As a result, Eq. (11) can be depicted by six

dimensionless π numbers (π_1 , π_2 , …, π_6) according to the Π theorem

$$f(\pi_1,\pi_2,\pi_3,\pi_4,\pi_5,\pi_6)=0 \tag{17}$$

Furthermore, according to Eqs. (16) and (17) can be expressed as

$$f(\theta,\frac{a}{b},\frac{h}{b},\frac{u_0}{\sqrt{bg}},\frac{\rho}{\rho_s},\frac{H}{b})=0 \tag{18}$$

The dimensionless expression for the run-up height of debris flows is derived as

$$\frac{H}{b}=\lambda_0(\frac{a}{b})^{\lambda_1}(\frac{h}{b})^{\lambda_2}(\mathrm{Fr}_1)^{\lambda_3}(\rho')^{\lambda_4} \tag{19}$$

3 Model tests

3.1 Test system

3.1.1 Debris flow modelling system

The physical model test platform of debris flows was divided into four zones: the source zone, the flowing zone, the interaction zone between debris flows and open flexible barriers, and the accumulation zone. The platform could reproduce the whole movement process of debris flows from initiation to flow, impact on flexible barriers, and accumulation, as displayed in Fig. 4. The source zone was a metal trough measuring 0.4 m in length, 0.3 m in width, 0.9 m in height, and 0.108 m^3 in volume. The flowing zone was a 4.2 m long, 0.3 m wide, and 0.5 m high flume, whose bottom was made of the perspex and side walls were made of the transparent toughened glass for the movement observation of debris flows, and the flume inclination varied from 20° to 40°. The accumulation zone was a metal platform with dimensions of 2.5 m×2.5 m (length× width), and it was used to record the topography characteristics of debris flows. The flexible barriers were positioned 0.5 m away from the flume end, i.e., the distance from the initiation position of debris flows to barriers was 3.7 m.

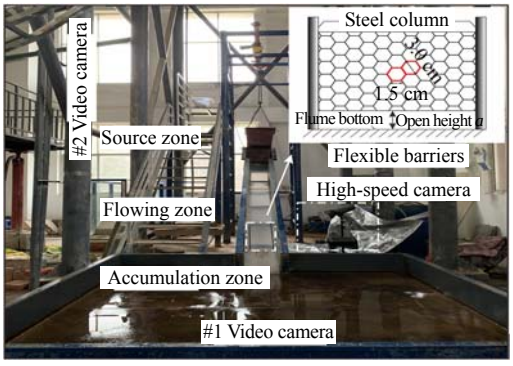

Fig. 4 Physical model equipment

3.1.2 Measurement system

The measurement system consisted of a high-speed camera, two video cameras, and a particle image velocimetry (PIV) device (Fig.5). The high-speed camera installed at the flume end was employed to record the movement processes of debris flows impacting the flexible barriers. The PIV device was employed to measure the velocities of debris flows before and after the barriers. The two video cameras mounted in front of the flume and above the accumulation platform were utilized to capture the trajectory and accumulation characteristics of debris flows rushing out of the flume.

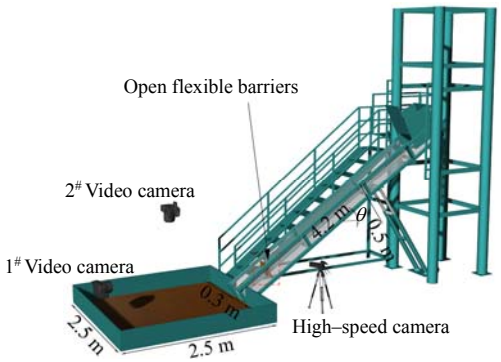

Fig. 5 Schematic diagram of the test system

3.2 Test material and design

The gradation curve of the debris flow grains used in the test[11] is plotted in Fig. 6, where the percentages of the grain with sizes of 40–60 mm, 20–40 mm, 10–20 mm, 5–10 mm, 2–5 mm, 1–2 mm, and 0.1–1.0 mm were 4.0%, 16.0%, 30.0%, 30.0.%, 15.5%, 2.5%, and 2.0%, respectively. The median grain size of debris flows $d_{50}=10$ mm and the characteristic grain size $d_{90}=30$ mm (Fig. 7). The barrier mesh adopted in the test was regular hexagonal, and the mesh size was determined as the d_{90} grain size ($b=3.0$ cm) (Fig. 4) by referring to the research findings about the mesh size selection of flexible barriers by Wendeler and Volkwein[6], Tan et al.[10], and Sun et al.[27]

Based on the results of the aforementioned dimensional analyses, the open height of flexible barriers, the relative density of debris flows, and the longitudinal slope of the gully were chosen as variables, and the velocity attenuation rate of debris flows, the run-up height of debris flows, and the blocking rate of flexible barriers were selected as evaluation indexes in the tests. Through the tests, the property parameters of debris flows (such as the relative density of debris flows, the time history of velocity, the flow depth, and the back siltation length) were yielded, and the regulation characteristics and laws of the relative open height of flexible barriers and the relative density of debris flows on debris flows were elaborated. The Froude number obtained from the physical model test was 3.8–6.8, which was consistent with the typical range of 0.5–7.6 according to the flume tests conducted by Choi et al.[28]. A total of 56 groups of tests were conducted, and the specific test schemes are shown in Table 2.

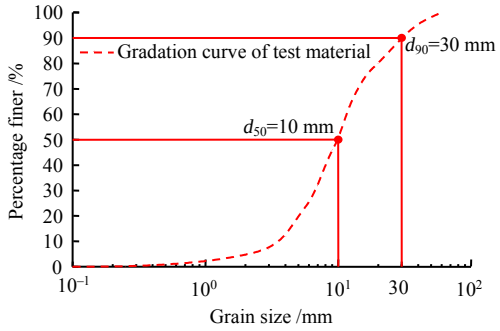

Fig. 6 Gradation curve of debris flow grain

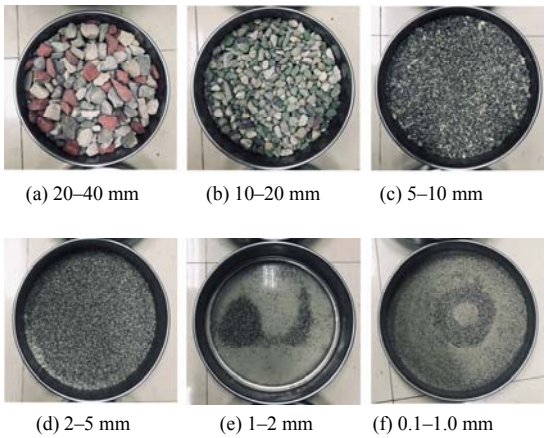

Fig. 7 Composition of debris flow grain size

Table 2 Test parameter design

Test group	Slope θ/(°)	Relative open height a/b	Relative density ρ'
1～24	25	0.00	0.60, 0.65, 0.70, 0.75
1～24	25	0.33	0.60, 0.65, 0.70, 0.75
1～24	25	0.50	0.60, 0.65, 0.70, 0.75
1～24	25	0.67	0.60, 0.65, 0.70, 0.75
1～24	25	0.83	0.60, 0.65, 0.70, 0.75
1～24	25	1.00	0.60, 0.65, 0.70, 0.75
25～44	30	0.00	0.60, 0.65, 0.70, 0.75
25～44	30	0.33	0.60, 0.65, 0.70, 0.75
25～44	30	0.50	0.60, 0.65, 0.70, 0.75
25～44	30	0.67	0.60, 0.65, 0.70, 0.75
25～44	30	0.83	0.60, 0.65, 0.70, 0.75
45～56	35	0.33	0.60, 0.65, 0.70, 0.75
45～56	35	0.50	0.60, 0.65, 0.70, 0.75
45～56	35	0.67	0.60, 0.65, 0.70, 0.75

3.3 Test results and analysis

3.3.1 Movement process analysis of debris flows impacting open flexible barriers

Taking the test where the slope $\theta = 30^\circ$ and the relative density $\rho' = 0.60$ as an example, the movement processes of debris flows impacting open flexible barriers for each condition were captured by a high-speed camera, as shown in Figs. 8(a)–8(e). Figure 8(c) shows the movement process of debris flows impacting open flexible barriers ($a/b = 0.50$), and the results demonstrated that: when $t = 0$ s, the head of debris flows reached the location 10 cm in front of the barriers, and the head velocity of the debris flows was 3.62 m/s; when $t =$ 0.33 s, the debris flows began to impact the flexible barriers, in which smaller sized debris flow particles directly passed through the opening below the flexible barriers and other debris flow particles climbed upward (shown by yellow arrows) to form the wedge siltation (shown by red arrows); when $t = 0.62$ s, the debris flows began to flow back in the opposite direction and interacted with the subsequent debris flows, and the energy was mostly dissipated at this stage; when $t = 1.60$ s, the debris flows passed through the flexible barriers at a speed of 2.69 m/s, which well reflects the self-cleaning effect of the open flexible barriers. Figures 9(a)–9(d) display the velocity vector fields of debris flows versus time during the operation of the closed flexible barriers ($a/b = 0$) (the location of the flexible barriers was the coordinate origin), and the debris flows interacted with the flexible barriers exhibited the movement characteristics of "flowing - climbing - backflow - accumulation". The difference in the debris flow velocities before and after the flexible barriers is evident, which further indicates that the flexible barriers can regulate the peak velocity of debris flows.

3.3.2 Shaving effect

The peak flow amount of debris flows is an essential indicator reflecting the scale and movement characteristics of debris flows, and the relationship between the debris flow velocity and the time (u–t curve) was chosen to indirectly represent the relationship between the flow amount and the time (q–t curve). To examine the regulation law of the open flexible barriers on the peak velocity of debris flows, the relative open height of flexible barriers and the relative density of debris flows were adopted as the influencing factors, and the velocity attenuation rate was chosen as the evaluation index. The velocity attenuation rate of debris flows is described as

$$R_a = (1 - \frac{u_1}{u_0}) \times 100\% \quad (20)$$

where u_1 is the debris flow velocity after the barriers (m/s).

Figures 10(a)–10(f) present the time histories of the debris flow velocity at 10 cm before and after the flexible barriers with varying open heights of the barriers (take $\theta = 25^\circ$ as an example). The peak velocity of debris flows after the barriers was lower than that before the barriers, and there were some differences in the peak shaving effect of the barriers with different open heights on the velocity–time curves. When the relative open heights were 1.00, 0.83, 0.67, 0.50, 0.33, and 0, the maximum velocity attenuation rates were 20.63%, 23.13%, 33.19%, 38.29%, 43.69%, and 53.91%, respectively, indicating that the peak shaving effect on the debris flows was more significant as the open height of flexible barriers decreased. However, a smaller open height could affect the self-cleaning ability of the flexible barriers.

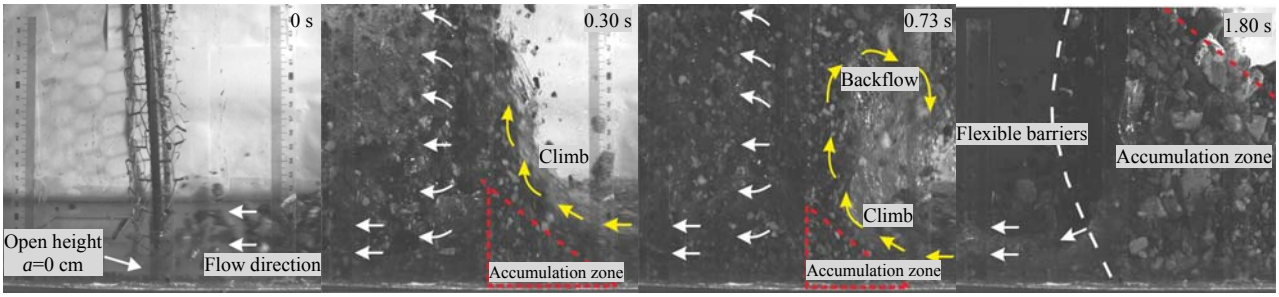

(a) $a / b = 0$

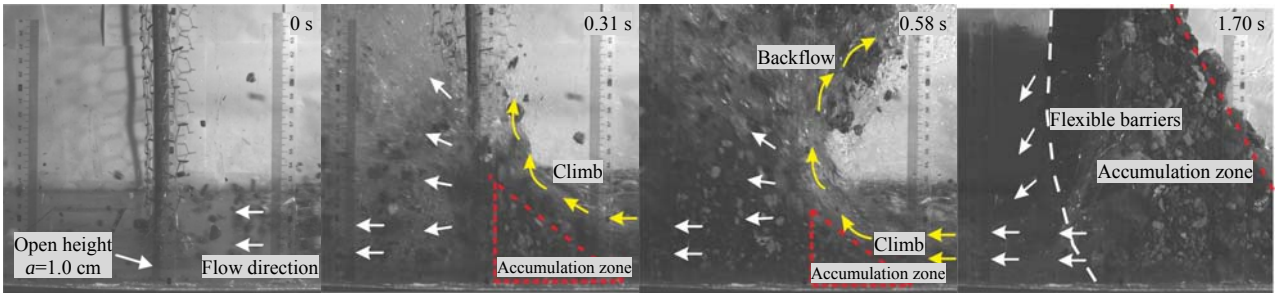

(b) $a / b = 0.33$

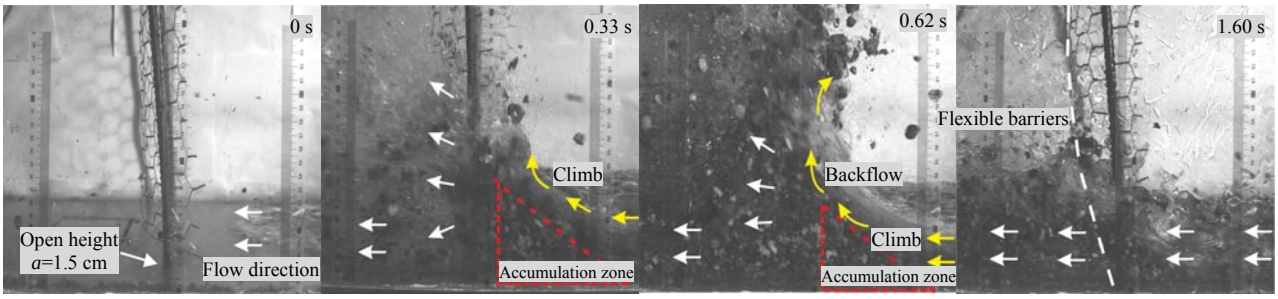

(c) $a / b = 0.50$

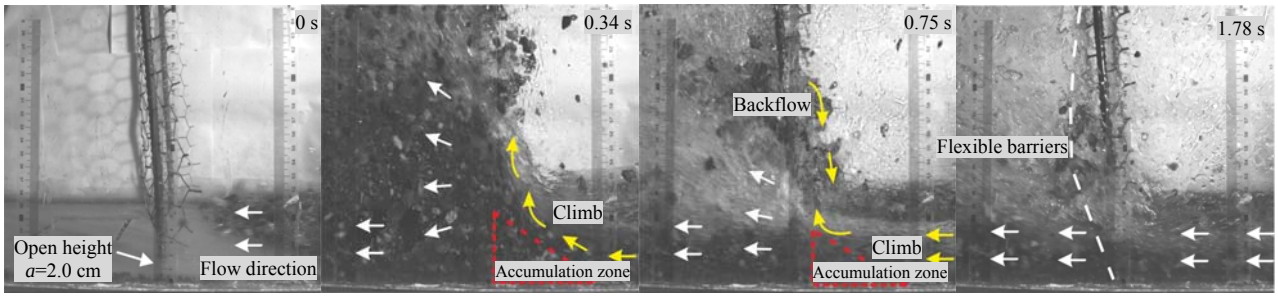

(d) $a / b = 0.67$

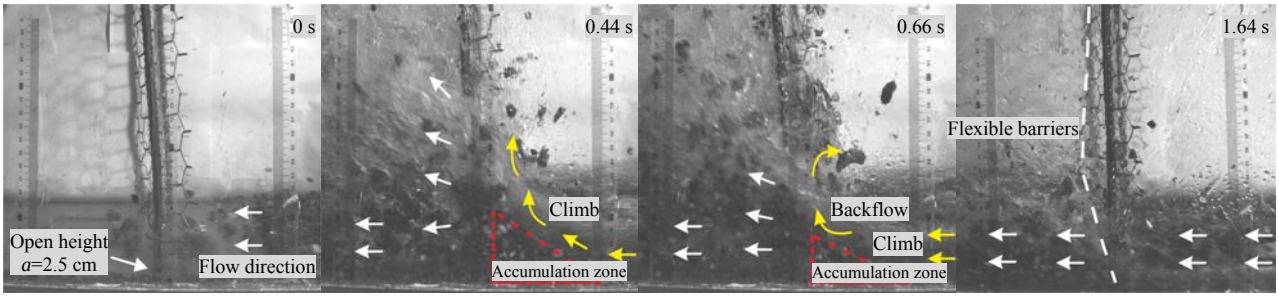

(e) $a / b = 0.83$

Fig. 8 Impact process of debris flows on flexible barriers at different open heights (θ=30°, ρ'=0.60)

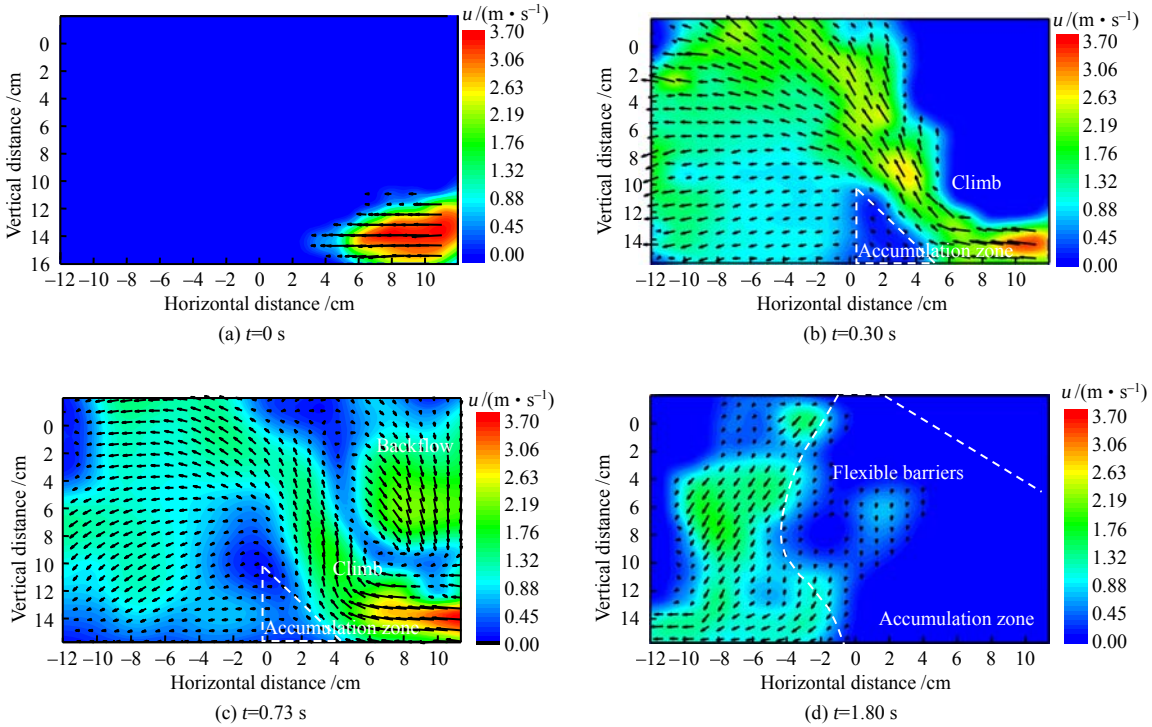

(a) t=0 s (b) t=0.30 s

(c) t=0.73 s (d) t=1.80 s

Fig. 9 Particle velocity fields of debris flow (a/b=0)

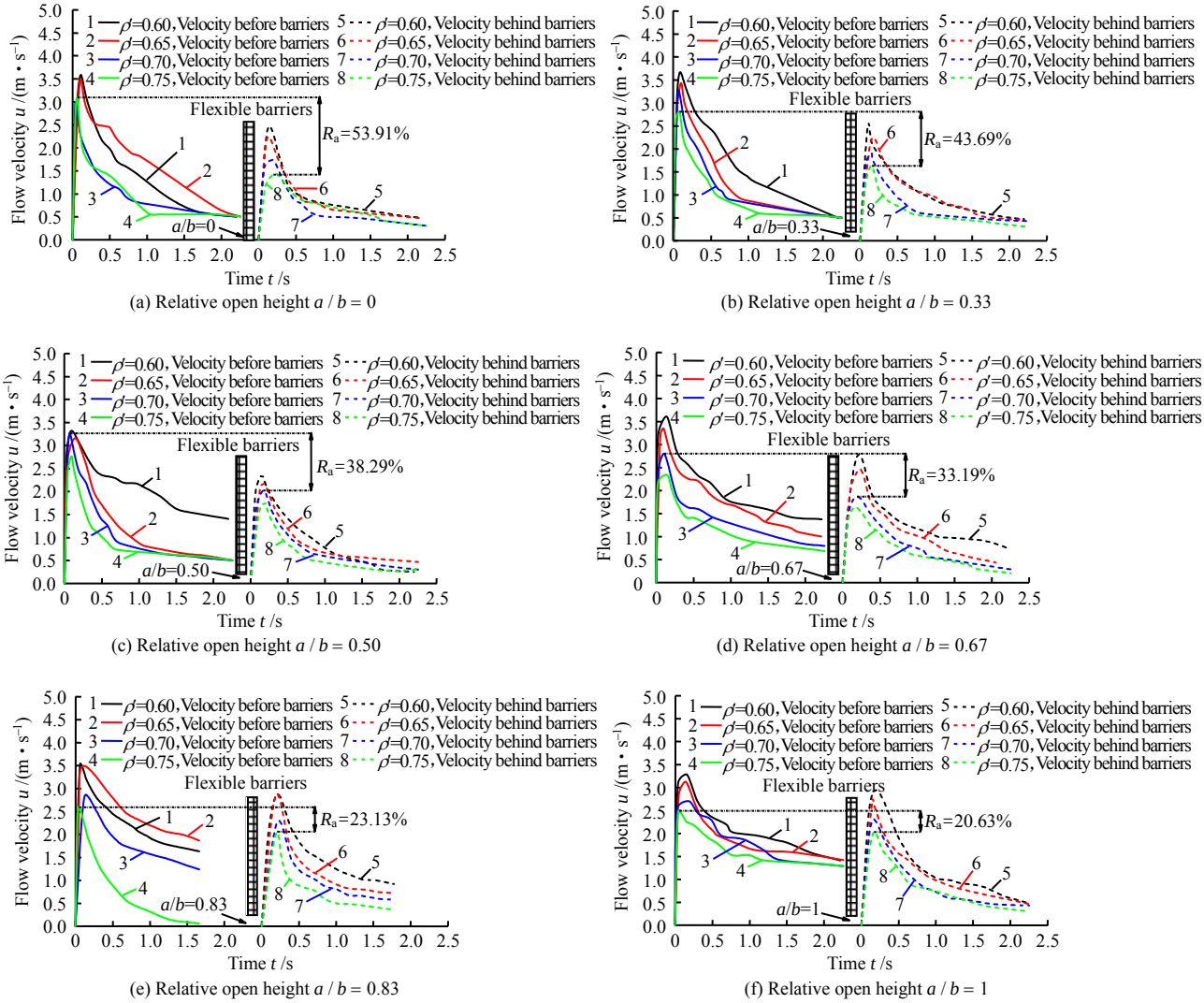

(a) Relative open height a / b = 0 (b) Relative open height a / b = 0.33

(c) Relative open height a / b = 0.50 (d) Relative open height a / b = 0.67

(e) Relative open height a / b = 0.83 (f) Relative open height a / b = 1

Fig. 10 Velocity–time curves of debris flows before and behind flexible barriers at different open heights (θ=25°)

Figure 11 depicts the correlation curve between the velocity attenuation rate R_a and the relative density ρ' of debris flows. The results revealed that the velocity attenuation rate increased with the increase of the relative density. Under the condition of $\rho' > 0.70$ and the relative open height being 0.50 and 0.67, the velocity attenuation rate of debris flows decreased slightly. In conjunction with Figs. 10(c) and 10(d), the reason why the velocity attenuation rate of debris flows decreased was considered as: as the relative density of debris flows increased, the influences of the viscosity of debris flows and the friction between the gully and the debris flows on the debris flow velocity were not negligible, which resulted in a significant decrease of the velocity of debris flows before the barriers and a low velocity attenuation rate. Based on Eq. (10) and the results of the flow velocity, the flow depth, and the velocity attenuation rate in the physical model tests, the empirical equations were established by the multiple nonlinear regression analysis, and the optimal solutions of the coefficients to be determined λ_0, λ_1, λ_2, λ_3, and λ_4 were determined as 0.246 5, −0.711 0, −0.212 7, 0.603 1, and 3.381 5. As a result, the relationships between the velocity attenuation rate R_a and the parameters, including the relative open height a/b, the dimensionless flow depth h/b, the Froude number Fr_1, and the relative density of debris flows ρ', is characterized as

$$R_a = 0.246\ 5\left(\frac{a}{b}\right)^{-0.711\ 0}\left(\frac{h}{b}\right)^{-0.212\ 7}(\mathrm{Fr}_1)^{0.603\ 1}(\rho')^{3.381\ 5} \tag{21}$$

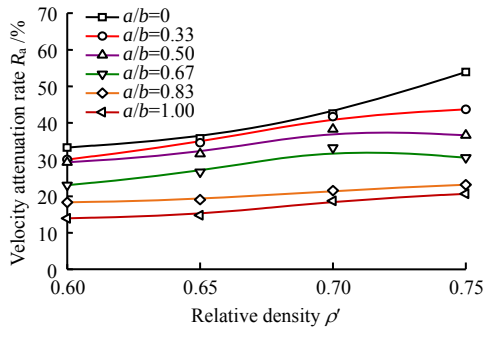

Fig. 11 Correlation between debris flow velocity attenuation rate and relative density (θ=25°)

The experimental and theoretical values of the velocity attenuation rate were compared (Fig. 12), and the results demonstrated that the correlation coefficient between the experimental and theoretical values of the velocity attenuation rate was 0.749, which was deemed a satisfactory fit.

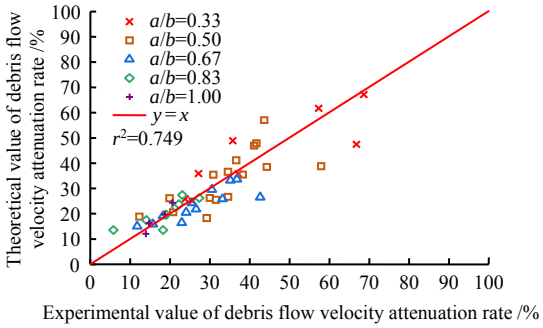

Fig. 12 Comparison of theoretical and experimental values of debris flow velocity attenuation rate

3.3.3 Self-cleaning effect analysis of open flexible barriers

The total overflow amount of debris flows and the total amount of solid materials pouring out at one moment are crucial indicators reflecting the scale of debris flows. The barrier engineering can be designed to trap part of the debris flows and reduce the risk of debris flows damaging the downstream infrastructures. However, a high debris flow blocking rate can block and destroy the flexible barriers, which makes the barriers lose their regulating capabilities. To explore the self-cleaning effect of flexible barriers, the relative open height of flexible barriers and the relative density of debris flows were selected as the influencing factors, and the blocking rate of flexible barriers was selected as the evaluation index. The equation of the blocking rate is

$$R_b = \frac{m_1}{m_0} \times 100\% \tag{22}$$

where R_b is the blocking rate of flexible barriers (%); m_0 is the total mass of the initially released debris flows (kg); and m_1 is the mass of the siltation before the flexible barriers (kg).

Figures 13 and 14 illustrate the final configurations of the siltation body of the debris flows with the relative open heights of flexible barriers of 0.33, 0.50, and 0.67 (take $\theta = 30°$ and $\rho' = 0.65$ as an example). The results revealed that the mass of the siltation, the length of the back siltation, and the height of the back siltation decreased with the increase of open height, and the blocking rates of flexible barriers fell in order of 42.31%, 21.03%, and 5.04%.

Figure 15 displays the correlation curves of the blocking rate of flexible barriers with the relative open height and the relative density of debris flows (take $\theta = 25°$ as an example), indicating that the relative open height and the relative density have a substantial influence on the blocking rate of flexible barriers. The

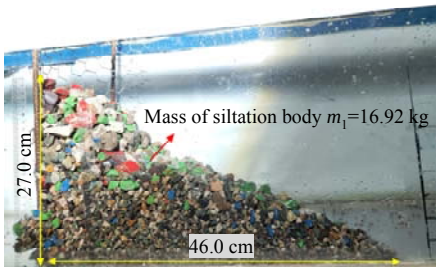

(a) Relative open height a / b = 0.33

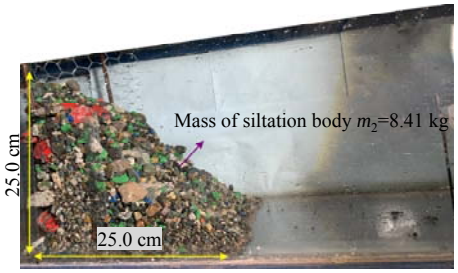

(b) Relative open height a / b = 0.50

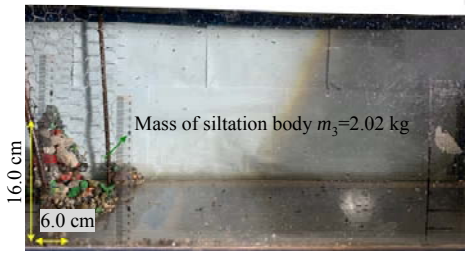

(c) Relative open height a / b = 0.67

Fig. 13 Configuration diagrams of siltation body at different open heights (θ=30°, ρ'=0.65)

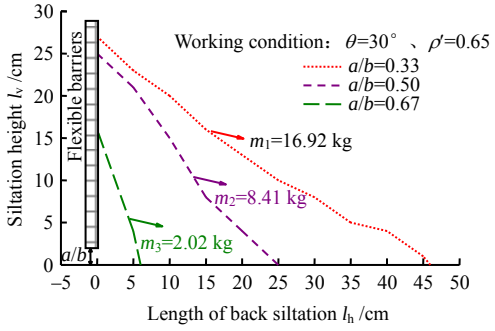

Fig. 14 Schematic diagram of siltation body configuration at different open heights(θ=30°, ρ'=0.65)

results revealed that the blocking rate decreased as the open height increased, but increased with the increase of the relative density. According to Fig. 15(a), the blocking rate of the open flexible barriers decreased dramatically when the relative open height reached 0.50. In order to fully use the self-cleaning effect of the open flexible barriers, the relative open height of flexible barriers in engineering design should be no less than 0.50. Given the impact and abrasion effects of debris flows on flexible barriers under real working conditions, it is recommended that double or even multiple layers of flexible barriers should be employed in practical engineering.

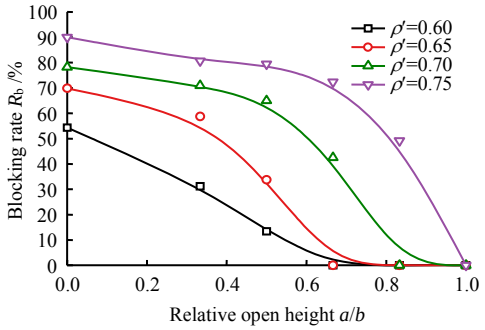

(a) Correlation curves between blocking rate and relative open height

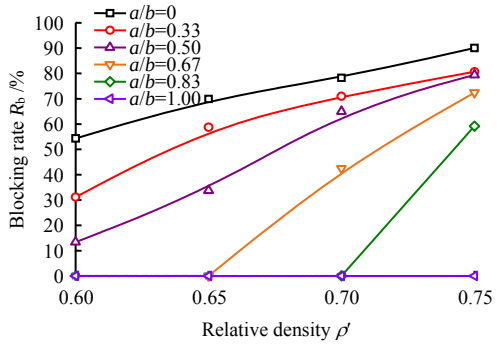

(b) Correlation curves between blocking rate and relative density

Fig. 15 Correlations between blocking rate and relative open height, relative density (θ=25°)

Based on Eq. (10) and the physical model test results of the flow velocity, the flow depth, and the blocking rate, the empirical equations were established by the multiple nonlinear regression analysis, and the optimal solutions for the coefficients to be determined λ_0, λ_1, λ_2, λ_3, and λ_4 were determined as 96.516 9, −2.530 7, −0.388 0, −2.073 1, and 10.097 1, respectively. Finally, the relationship between the blocking rate and the parameters, including the relative open height a/b, the dimensionless flow depth h/b, the Froude number Fr_1, and the relative density of debris flow ρ', is described as

$$R_b = 96.516\,9\left(\frac{a}{b}\right)^{-2.530\,7}\left(\frac{h}{b}\right)^{-0.388\,0}(\mathrm{Fr}_1)^{-2.073\,1}(\rho')^{10.097\,1} \tag{23}$$

The experimental and theoretical values of the blocking rate were compared (Fig. 16), and the results demonstrated that the correlation coefficient r^2 between the experimental and theoretical values of the blocking rate of the opening flexible barriers was 0.712.

3.3.4 Run-up height analysis of debris flows upon open flexible barriers

The correlation curves between the run-up height of debris flows and the open height of flexible barriers under various densities of debris flows and a/b are shown in Fig. 17. The results revealed that the run-up height of debris flows decreased with the increase of both the relative open height and the relative density.

The change rate of the run-up height of debris flows was 25.9% when $\rho'=0.65$, and 38.5% when $a/b=0.50$. Therefore, the increases of both the relative open height of flexible barriers and the relative density can reduce the run-up height of debris flows to some extent, but the run-up height of debris flows is more sensitive to changes in the relative density of debris flows.

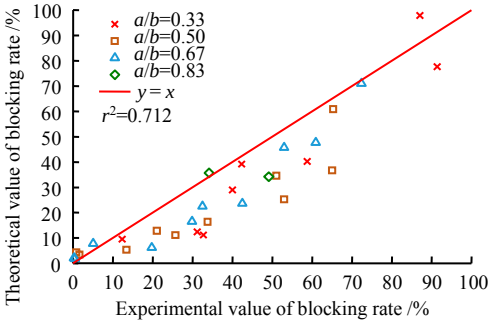

Fig. 16 Comparison of theoretical and experimental values of the blocking rate

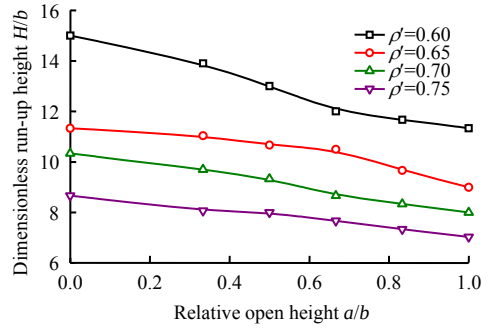

(a) Correlation curves between run-up height and relative open height

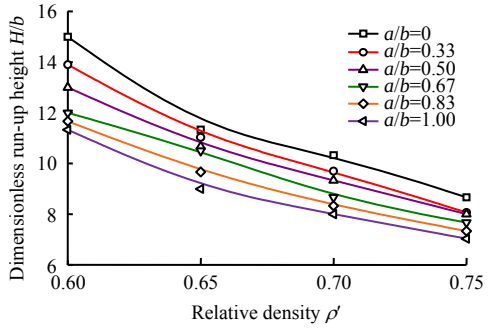

(b) Correlation curves between run-up height and relative density

Fig. 17 Correlations between run-up height of debris flow and relative open height, relative density (θ=25°)

Based on Eq. (19) and the results of the flow velocity, the flow depth, and the run-up height in the physical model tests, the empirical equations were established by the multiple nonlinear regression analysis, and the optimal solutions of the coefficients to be determined under the dimensionless run-up height were 3.529 8, −0.036 9, 0.094 1, 0.100 2, −1.945 6, respectively. Finally, the relationship between the dimensionless run-up height H/b and the parameters, including the relative open height a/b, the dimensionless flow depth h/b, the Froude number Fr_1, and the relative density of debris flows ρ', is characterized as

$$\frac{H}{b}=3.529\ 8\left(\frac{a}{b}\right)^{-0.036\ 9}\left(\frac{h}{b}\right)^{-0.094\ 1}(\mathrm{Fr}_1)^{-0.100\ 2}(\rho')^{-1.945\ 6} \tag{24}$$

The experimental and theoretical values of the dimensionless run-up height were compared (Fig. 18), and the results showed that the correlation coefficient r^2 between the experimental and theoretical values of the dimensionless run-up height of debris flows values was 0.803, indicating a good agreement between the experimental and theoretical values.

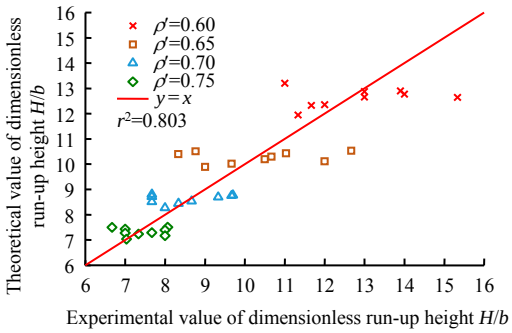

Fig. 18 Comparison of theoretical and experimental values of debris flow run-up height

4 Conclusions

The open flexible barriers used for debris flow mitigation were first proposed, the regulation performance of the open flexible barriers on debris flows was then investigated through theoretical analyses and physical model tests. The theoretical formulas for the velocity attenuation rate of debris flows, the run-up height of debris flows, and the blocking rate of flexible barriers were finally established. The major findings are summarized as follows:

(1) The debris flows show the movement characteristics of "flowing-climbing-backflow-flowing (accumulation)", when they interact with open flexible barriers. Compared with the closed flexible barriers, the open flexible barriers have a good self-cleaning ability, can effectively regulate the velocity curve of debris flows, and can reduce the peak velocity of debris flows.

(2) The physical model test results demonstrate that: the velocity attenuation rate of debris flows decreases with the increasing open height, and the velocity attenuation rate increases with the increasing

relative density under the same open height; and the blocking rate of flexible barriers is negatively correlated with the open height. When the open height is fixed, the blocking rate is positively correlated with the relative density; the run-up height is negatively correlated with both the relative open height and the relative density, and the influence of the density of debris flows on the run-up height is more significant than that of the open height.

(3) The formulas for calculating the velocity attenuation rate of debris flows, the blocking rate, and the run-up height using the open height a/b, the dimensionless flow depth h/b, the relative density of debris flows ρ', and the Froude number Fr_1 are obtained through dimensional analyses, and the above formulas are quantitatively verified by physical model tests. The results of the theoretical formulas correspond well with the physical test results, indicating that the formulas can be applied to the design of open flexible barriers.

(4) The open flexible barriers are suitable for preventing debris flows in high or narrow steep gullies with a river width less than 30 m. The open flexible barriers have the advantages and characteristics such as the self-cleaning ability, intercepting boulders or reducing the speed of boulders, low cost, and environmental friendliness. However, before the open flexible barriers are applied in the practical engineering, the structure and the depth design of the anchorage fixed on both sides of the gully need to be further addressed. The authors will further improve the open flexible barriers in specific engineering applications.

References

[1] YU Zhi-xiang, ZHANG Li-jun, LUO Li-ru, et al. Study on impact resistance of a resilient steel canopy protection system[J]. Chinese Journal of Rock Mechanics and Engineering, 2020, 39(12): 2505–2516.

[2] ZHAO Shi-chun, YU Zhi-xiang, ZHAO Lei, et al. Damage mechanism of rockfall barriers under strong impact loading[J]. Engineering Mechanics, 2016, 33(10): 24–34.

[3] HE Yong-mei, CHENG Ming. Research on the application of flexible system to mitigation of mudflow[J]. Research of Soil and Water Conservation, 2007, 14(3): 292–294, 299.

[4] XIE Tao, XU Xiao-lin, CHEN Hong-kai. Review and trends on debris dam research[J]. The Chinese Journal of Geological Hazard and Control, 2017, 28(2): 137–145.

[5] LIU Cheng-qing, XU Cheng-jie, CHEN Xin, et al. Failure cause analysis and countermeasures design of flexible debris flow protection system[J]. Journal of Water Resources and Architectural Engineering, 2017, 15(5): 6–11.

[6] WENDELER C, VOLKWEIN A. Laboratory tests for the optimization of mesh size for flexible debris-flow barriers[J]. Natural Hazards and Earth System Sciences, 2015, 15(12): 2597–2604.

[7] KWAN J S H, CHAN S L, CHEUK J C Y, et al. A case study on an open hillside landslide impacting on a flexible rockfall barrier at Jordan Valley, Hong Kong[J]. Landslides, 2014, 11(6): 1–14.

[8] WENDELER C, VOLKWEIN A, MCARDELL B W, et al. Load model for designing flexible steel barriers for debris flow mitigation[J]. Canadian Geotechnical Journal, 2019, 56(6): 893–910.

[9] VOLKWEIN A, WENDELER C, GUASTI G. Design of flexible debris flow barriers[C]//In 5th International Conference Debris-flow Hazard Mitigation, Mechanics, Prediction and Assessment. Padua: [s. n.], 2011: 1093–1100.

[10] TAN D Y, YIN J H, QIN J Q, et al. Experimental study on impact and deposition behaviours of multiple surges of channelized debris flow on a flexible barrier[J]. Landslides, 2020, 17(7): 1577–1589.

[11] WANG Dong-po, ZHANG Xiao-mei, Dynamic response research of debris flow impact arc-shaped dam[J]. Rock and Soil Mechanics, 2020, 41(12): 3851–3861.

[12] ARMANINI A, ROSSI G, LARCHER M. Dynamic impact of a water and sediments surge against a rigid wall[J]. Journal of Hydraulic Research, 2019, 58(2) 314–325.

[13] SONG D, CHOI C E, NG C W W, et al. Geophysical flows impacting a flexible barrier: effects of solid-fluid interaction[J]. Landslides, 2017, 15(1): 99–110.

[14] LI Jun-jie, WANG Xiu-li, RAN Yong-hong. Experimental study dynamic response of a new dam to the impact of block stones in debris flow[J]. Journal of Harbin Engineering University, 2018, 39(5): 94–101.

[15] REN Gen-li, WANG Xiu-li. Simulation study on the response the composite structure with steel strand network impacted by debris flow boulders[J]. Safety and Environmental Engineering, 2019, 26(5): 89–97.

[16] WANG Xiu-li, QIAO Fen, RAN Yong-hong, et al. Dynamic response analysis for a new type of debris flow flexible protection system[J]. The Chinese Journal of Geological Hazard and Control, 2018, 29(5): 114–121.

[17] LI X, ZHAO J. A unified CFD-DEM approach for modeling of debris flow impacts on flexible barriers[J]. International Journal for Numerical and Analytical Methods in Geomechanics, 2018, 42(14): 1643–1670.

[18] LI S, YOU Y, CHEN X, et al. Regulation effectiveness of a window-check dam on debris flows[J]. Engineering Geology, 2019, 253: 205–213.

[19] SUN H, YOU Y, LIU J, et. al. Experimental study on discharge process regulation to debris flow with open-type check dams[J]. Landslides, 2021, 18(3): 967–978.

[20] WANG Xiao-jun, CHEN Xiao-qing, XIE Xiang-ping, et al. The optimization of debris flow check dam drainage hole and its numerical simulation research[J]. Science Technology and Engineering, 2016, 16(9): 28–34.

[21] YU Xian-bin, CHEN Xiao-qing, ZHAO Wan-yu, et al. Influence of the perforated parameters of permeable dam drain hole on the dam stress field[J]. Journal of Disaster Prevention and Mitigation Engineering, 2016, 36(6): 1015–1025.

[22] ZHAO Guo-yan, LIANG Wei-zhang, WANG Shao-feng, et al. Prediction model for extent of excavation damaged zone around roadway based on dimensional analysis[J]. Rock and Soil Mechanics, 2016, 37(Suppl.2): 273–278, 300.

[23] YAO Nan, YE Yi-cheng, WANG Qi-hu, et al. Study on influence of stability of gently inclined stope roof based on dimensional analysis[J]. Rock and Soil Mechanics, 2018, 39(11): 4232–4241.

[24] LIN Lan, LI Sa, SUN Li-qiang, et al. Study of relative compaction for calcareous sand soil using dynamic cone penetration test[J]. Rock and Soil Mechanics, 2020, 41(8): 2730–2738.

[25] ZHAO Kang, ZHAO Kui, SHI Liang. Collapsing height prediction of overburden rockmass at metal mine based on dimensional analysis[J]. Rock and Soil Mechanics, 2015, 36(7): 2021–2026.

[26] NG C W W, MAJEED U, CHOI C E, et al. New impact equation using barrier Froude number for the design of dual rigid barriers against debris flows[J]. Landslides, 2021, 18(6): 1–13.

[27] SUN Hao, YOU Yong, LIU Jin-feng. Experimental study on regulative performance of debris flow beam dam[J]. Journal of the China Railway Society, 2019, 41(3): 163–168.

[28] CHOI S K, LEE J M, KWON T H. Effect of slit-type barrier on characteristics of water-dominant debris flows: small-scale physical modeling[J]. Landslides, 2018, 15(1): 111–122.